J. Am. Soc. Mass Spectrom. (2016) 27:2014–2024
DOI: 10.1007/s13361-016-1492-z

RESEARCH ARTICLE

Reducing the Matrix Effect in Organic Cluster SIMS Using Dynamic Reactive Ionization

Hua Tian,[1] Andreas Wucher,[2] Nicholas Winograd[1]

[1]Chemistry Department, The Pennsylvania State University, University Park, PA 16802, USA
[2]Fakultät für Physik, Universität Duisburg - Essen, 47048, Duisburg, Germany

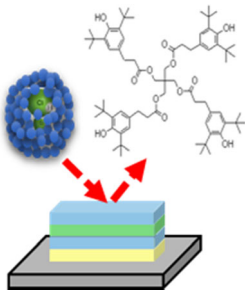

Abstract. Dynamic reactive ionization (DRI) utilizes a reactive molecule, HCl, which is doped into an Ar cluster projectile and activated to produce protons at the bombardment site on the cold sample surface with the presence of water. The methodology has been shown to enhance the ionization of protonated molecular ions and to reduce salt suppression in complex biomatrices. In this study, we further examine the possibility of obtaining improved quantitation with DRI during depth profiling of thin films. Using a trehalose film as a model system, we are able to define optimal DRI conditions for depth profiling. Next, the strategy is applied to a multilayer system consisting of the polymer antioxidants Irganox 1098 and 1010. These binary mixtures have demonstrated large matrix effects, making quantitative SIMS measurement not feasible. Systematic comparisons of depth profiling of this multilayer film between directly using GCIB, and under DRI conditions, show that the latter enhances protonated ions for both components by 4- to ~15-fold, resulting in uniform depth profiling in positive ion mode and almost no matrix effect in negative ion mode. The methodology offers a new strategy to tackle the matrix effect and should lead to improved quantitative measurement using SIMS.

Keywords: Ar gas cluster ion beam, Dynamic reactive ionization, Secondary ion mass spectrometry, Depth profiling, Matrix effect, Irganox

Received: 4 July 2016/Revised: 24 August 2016/Accepted: 25 August 2016/Published Online: 22 September 2016

Introduction

A significant obstacle to utilize secondary ion mass spectrometry (SIMS) as a quantitative tool for materials characterization has been the observed variation of the ionization probability of the target molecule with local environment. This variation, euphemistically described as the "SIMS matrix effect" [1], can result in changes in signal intensity of many orders of magnitude. There has been mixed success at controlling this effect for inorganic samples by, for example, oxygen flooding [2], composition matching [3], and the use of internal standards [4]. Results are more problematic for organic compounds where the ionization mechanism often involves protonation or other charge transfer processes [5]. This class of compounds is now particularly important because of a growing focus on organic electronics [6], bioimaging [7], and molecular depth profiling [8–10], applications made possible by the emergence of primary ions consisting of various molecular clusters, such as SF_5^+, C_{60}^+, and Ar_n^+ (n = 1000–10,000) [11–14].

The SIMS matrix effect for organic compounds can be severe since the ionization probability for most molecules is a rare event, generally fewer than 1 in 10,000 [15]. Hence, charge exchange processes resulting in ion suppression or enhancement can exert an enormous effect upon the secondary ion yield. There have been recent attempts to develop a strategy to better understand and characterize the variations. The National Physical Laboratory (NPL) in the U. K. developed a complex multilayer reference material that has been subjected to a Versailles Project on Advanced Materials and Standards (VAMAS) round-robin study [5]. The results show that the largest matrix effects are observed when detecting higher mass species than lower mass species, and when employing larger primary ion clusters such as Ar_{3000}^+ than smaller ones such as Bi_3^+. The severe matrix effects observed for the gas cluster ion sources (GCIB) are particularly problematic since these clusters generally produce mass spectra with the least amount of fragmentation and yield the best depth resolution during

Electronic supplementary material The online version of this article (doi:10.1007/s13361-016-1492-z) contains supplementary material, which is available to authorized users.

Correspondence to: Hua Tian; *e-mail:* hut3@psu.edu

molecular depth profiling [5]. To address this concern, a water cluster ion source has been developed, with the aim of delivering an excess of protons to the impact area, a concept that has indeed reduced the magnitude of the matrix effect and enhanced the ion yield [16].

Our approach to this problem has been to develop a strategy referred to as dynamic reactive ionization (DRI) [17]. With this approach, the GCIB is doped with a few percent of HCl. In the presence of H_2O, the formation of H_3O^+ and Cl^- is energetically favored and provides another pathway to deliver protons to the cluster impact site. The H_2O is introduced by leaking it into the mass spectrometer, followed by condensation onto the cold sample surface (100 K) at an optimized rate, creating a favorable surface environment for the dissociation of HCl. In previous studies, we have shown that the ionization probability can be increased by more than an order of magnitude, reaching levels comparable to those produced by the H_2O cluster ion source or by a C_{60}^+ ion source. Moreover, DRI has been shown to reduce salt suppression of molecular ions in complex biological tissue [18].

In this work, the DRI strategy is applied to characterization of a multilayer organic thin film of mixed composition, consisting of pure polymer antioxidants Irganox 1010 and Irganox 1098 layer and their mixed layers. The multilayer film is similar to the NPL reference material employed in the VAMAS study discussed above. The results show that the protonated molecular ion, $[M + H]^+$ is greatly enhanced by 4- to ~10-fold for both components in the thin film, leading to uniform depth profiling, which can be interpreted in a quantitative manner in positive ion mode, while almost no matrix effect was observed during the entire depth profile in negative ion mode compared with non-DRI conditions.

Experimental

Materials

Trehalose films were prepared by spin-coating of a trehalose solution onto a Si substrate. D- (+)-trehalose dehydrate (BioReagent; Sigma, Milwaukee, WI, USA) was dissolved into HPLC water at concentration of 0.5 M. An aliquot of 100 μL of the 0.5 M solution was spin- coated (Laurell, WS-650MZ-23NPP/UD2, North Wales, PA, USA) onto a pre-cleaned Cu wafer (sonicated in chloroform, HPLC water, and methanol for 5 min, respectively) at 4000 rpm, resulting in a uniform film of ~200 nm in thickness [19].

The multilayer Irganox1010/Irganox1098 samples were purchased from NPL, UK. The film was deposited onto finely polished Si or Cu substrates (9.5 mm × 9.5 mm, 0.5 mm thickness) with the layer sequence as shown schematically in Supplementary Figure S1, consisting of 100 nm thick Irganox 1098, 50% Irganox 1010:50% Irganox 1098 mixture, Irganox 1010, and Irganox 1098 layers, respectively, refereed as layer 1 to 4 in the following. In order to simplify the discussion, the two components will be referred as "1098" and "1010", respectively. The thickness of each layer was monitored during the deposition process at NPL by a quartz crystal microbalance calibrated by spectroscopic ellipsometry. The composition of the mixed layer was confirmed at NPL by XPS and Ar cluster sputter depth profiling [20].

SIMS Measurement

The concept of DRI to enhance the protonation probability of sputtered molecules has been described in detail elsewhere [17]. Briefly, a hybrid Ar cluster projectile is formed by mixing the reactive species, HCl in this case, into the backing gas driving the supersonic expansion. HCl is hydrolyzed at the cluster impact site in the presence of H_2O, yielding the free hydronium ion, H_3O^+, to assist the protonation of molecules. In the experiments described here, we use a premixed gas of 10% HCl in Ar (Praxair, Toledo, OH, USA), which is further diluted with pure Ar gas to achieve the desired HCl content. The gas mixture was then used to operate a 20 keV gas cluster ion source (GCIB 20; Ionoptika, Southampton, UK) at a backing pressure of 18 bar. Throughout the experiments, the HCl content in the backing gas was varied between 1.25% and 5%. As shown in our previous experiments with mixed cluster beams, we expect the actual HCl content of the projectile cluster ions to be higher [21]. HCl doped Ar_n^+ cluster ions with a size distribution centered around n = 2000–3000 atoms and a half width of ~±900 atoms were selected for this study, abbreviated as Ar_n^+ (x% HCl) in the following discussion. The currents of the mixed cluster ion beam were between 50 and 150 pA depending upon the HCl dopant level.

The depth profiling experiments were accomplished using a J105 3D Chemical Imager by Ionoptika, UK [22] by simultaneous acquisition of a sequence of images and sputter erosion with the ion beam rastered over the analysis area. The ion beam was operated in a pulsed mode with varying duty cycles in order to avoid excessive charging of the surface. The ion fluence accumulated during each of these imaging cycles (in the following referred to as "layers") was of the order of 5×10^{-2} ions/nm^2. Precaution was taken to make sure that the ion beam spot size on the sample was larger than the image pixel size, thereby ensuring a homogeneous fluence distribution across the raster area. During the depth profile, H_2O was introduced into the analysis chamber by means of a controllable leak valve connected to a vial containing water when the sample stage was cooled to 100 K. The water pressure was monitored using a residual gas analyzer (Spectra, Morgan Hill, CA, USA) and recorded through the entire measurement.

The J105 instrument features a Daley type ion detector, which records the signal using an 8 bit transient digitizer (Ortec FastFlight II; Oak Ridge, TN, USA). Therefore, the recorded flight time spectrum represents the ion signal in somewhat arbitrary digitizer units, which will in the following plots be displayed on the signal intensity scale. Experiments comparing the FastFlight output to the ion count rate measured by a time-to-digital converter have revealed that the FastFlight output must be divided by a factor of the order of 60 in order to arrive at the true detected ion counts. In order to be able to compare

signal levels obtained in different experiments, the measured mass peak integral (in arbitrary digitizer units) is normalized by the primary ion current (in pA) and an arbitrary constant of 10^3.

Our previous DRI study performed on trehalose films suggested that the higher signal intensity induced by the projectile assisted surface chemistry can be dynamically controlled and maintained during depth profiling by finely adjusting the background partial pressure of D_2O water vapor in the analysis chamber [17]. In these experiments, it was found that the chemical reaction between HCl entrained in the projectile and the D_2O molecules adsorbed on the surface lead to H/D exchange reactions within the sputtered molecules, thereby greatly complicating the measured mass spectra. Based upon these results, we further tested the feasibility of the DRI approach to perform actual depth profiling using H_2O instead of D_2O and maintaining a constant H_2O partial pressure after the initial establishment of optimum ionization conditions.

During the trehalose experiment, an Ar_{1500}^+ (5% HCl) ion beam was rastered across an area of 200 × 200 μm^2 with 32 × 32 pixels at a dose of 8×10^{-2} ions/nm^2 for each layer on the trehalose film at 100 K. In these initial experiments, the H_2O pressure was gradually increased after the start of a depth profile in order to reach the maximum signal of protonated trehalose molecules and then kept at that optimum value of 6 ~8×10^{-7} mbar, until the trehalose film was etched away and the interface to the underlying Cu substrate was reached. The signal intensities of the molecule-specific secondary ions $[M - OH]^+$, $[M + H]^+$, $[M + Na]^+$, and $[2M + H]^+$ (where M refers to the intact trehalose molecule at $m/z = 342$) at m/z 325, 343, 365, and 685 were monitored along with a water cluster ion $[(H_2O)_5H]^+$ at m/z 91.

The further application of DRI depth profiling was performed to investigate the matrix effect in NPL Irganox1010/Irganox1098 multilayer film. Depth profiling of this sample was performed using an Ar_{3000}^+ (1.25% HCl) projectile ion beam at 100 K. The beam was rastered over an area of 300 × 300 μm^2 with 32 × 32 pixels at a dose around 5×10^{-2} ions/nm^2 depending upon the value of the primary ion current. The H_2O partial pressure was adjusted to 2×10^{-7} mbar (except where otherwise stated) at the beginning of the depth profile and monitored during the entire depth profile. In addition, the secondary ion signal of water cluster ions $(H_2O)_nH^+$ or $(H_2O)_nOH^-$ (n =10, 11) was monitored to ensure that the buildup of an excessive ice layer at the surface was avoided. For comparison, depth profiles were recorded using different projectiles under different conditions, as in the following, A, 40 keV C_{60}^+ projectile without H_2O flooding; B, Ar_{3000}^+ projectile without H_2O flooding; C, Ar_{3000}^+ (1.25% HCl) projectile without H_2O flooding; D, Ar_{3000}^+ projectile with H_2O flooding.

The depth profiles were recorded both in positive and negative secondary ion mode. In both modes, it was found that compensation of surface charging induced by the ion bombardment is extremely important in order to obtain reproducible results. The first precaution was taken by mounting the sample underneath a stainless steel grid of 0.1 mm thickness with 1 mm mesh width, and each depth profile was acquired on a fresh sample area in the center of a new grid. In positive ion mode, charge compensation was performed by co-bombarding the surface with a defocused 10 eV He^+ ion beam at a total current of about 3 μA in order to avoid the negative surface charge induced by the high total secondary ion yield. In negative ion mode, an electron flood gun was used at 20 eV electron energy delivering a defocused beam of about 1 nA current in order to compensate for positive charge induced by high secondary ion and electron yields. In some cases, particularly in the negative ion mode, both the He^+ and the electron beam were used simultaneously in order to provide compensation for charging in either direction.

Sputter Rate Measurement

In order to determine the total film thickness along with possible variations of the erosion rate between different layers, a wedge crater was eroded into the Irganox multilayer sample. The process used to erode such craters is described in detail elsewhere [23–25]. Briefly, the sample surface was eroded using the Ar_{3k}^+ projectile ion beam operated in DC mode and rastered across an area of 500 × 500 μm^2 with 128 × 128 pixel within 128 frames and a pixel dwell time of about 20 μs. In each frame, one more line is skipped from the raster, leading to a linear increase of the applied ion fluence between zero and its maximum value from one side to the other side of the crater. The frame set was then repeated until the substrate was reached on the deep side of the crater. The wedge crater was then profiled by a wide scan range atomic force microscope (AFM) (NPX200; Seiko Instruments Inc., Iwate, Japan) in order to determine the erosion rate at different depth of the sample.

Results and Discussion

Synopsis

This section is organized as follows. First, we investigate the merits of the DRI scheme by comparing the useful molecular ion yield determined on trehalose films with those obtained under "normal" molecular depth profiling conditions using other cluster projectiles. We then present the first complete DRI depth profile of an entire film, which was obtained on this system using an HCl doped Ar GCIB in combination with simultaneous H_2O adsorption. In order to investigate the influence of the DRI modality on the matrix effect often observed in multicomponent organic molecular depth profiles, we then switch to the Irganox multilayer system and compare molecular depth profiles taken with the pure and HCl doped Ar GCIB alone and under H_2O dosing conditions, respectively.

1. Trehalose In order examine the prospects of molecular depth profiling under DRI conditions, trehalose was investigated as a model system since it has been employed in our previous study [17] introducing the reactive ionization mechanism as a means of enhancing molecular ion intensities via $[M + H]^+$ ion

formation. The depth profile of a 200-nm-thick film of trehalose under DRI conditions, which employs 20 keV Ar_{1500}^+ (5% HCl) cluster ion beam with simultaneous introduction of water vapor into the analysis chamber, is shown in Figure 1. A more detailed plot of all relevant recorded signals is shown in the Supporting Figure S2. In the beginning of the profile, the H_2O partial pressure was gradually increased, until after removal of about 60 layers nearly optimum conditions for $[M + H]^+$ formation were reached. As already demonstrated [21], this situation is characterized by an overshoot of the $[M + H]^+$ ion signal over the $[M – OH]^+$ and $[M + Na]^+$ ion signal. Under "normal" depth profiling conditions (pure Ar cluster beam and dry surface), the $[M – OH]^+$ ion clearly dominates the spectrum. After that, the H_2O partial pressure was held constant, leading to steady state signal levels of the molecule specific $[M + H]^+$ and $[M – OH]^+$ ions. As seen from the water cluster ion signal at *m/z* 91, however, the H_2O surface coverage still kept gradually increasing, leading to a further suppression of the $[M – OH]^+$ fragment and particularly the $[M + Na]^+$ salt adduct ions, while the $[M + H]^+$ signal stayed constant or even slightly increased. This profile shows that these optimum conditions can be dynamically maintained throughout the removal of the remaining film until the copper substrate is reached. Here, the $[M + H]^+$ ion exhibits a steep decay as expected, while the other two molecule-specific ions exhibit pronounced interface maxima, which strongly deteriorates the depth resolution. From these observations, we conclude that it is in principle possible to establish and maintain DRI conditions throughout a molecular depth profile.

In order to judge the prospects of DRI with respect to protonation enhancement, it is of interest to compare useful yields (i.e., the probability that a molecule removed from the surface by sputtering is being detected as a protonated molecular ion). Trehalose films have been investigated by many laboratories as a reproducible testing platform for molecular depth profiling experiments, and therefore one can deduce useful yields for the molecule-specific ions of this material obtained under bombardment with practically all different cluster projectiles that are now routinely being used in molecular SIMS depth profiling. The results are compiled in Table 1, which shows useful yield values calculated from published ToF-SIMS data as indicated in the table. In order to arrive at the displayed values, the molecule-specific secondary ion signal measured at the beginning of the depth profile was divided by the number of sputtered molecule equivalents removed. The latter is given as the product of the ion fluence applied to acquire the spectrum, the sputter yield (in molecules per ion), and the raster area of the ion beam during spectrum acquisition. The sputter yield was determined from the ion fluence needed to remove a film of given thickness, using the molecule density of trehalose of 2.7 molecules/nm^3. Although the data underlying the values in Table 1 were acquired using different instruments exhibiting, in principle, different transmission and detection probability for the secondary ions, this difference was disregarded in the compilation. The magnitude of the resulting deviation was checked by comparing data tabulated for the same projectile obtained on different instruments and was found to be small enough that at least the order of magnitude of the tabulated useful yield values remains unchanged.

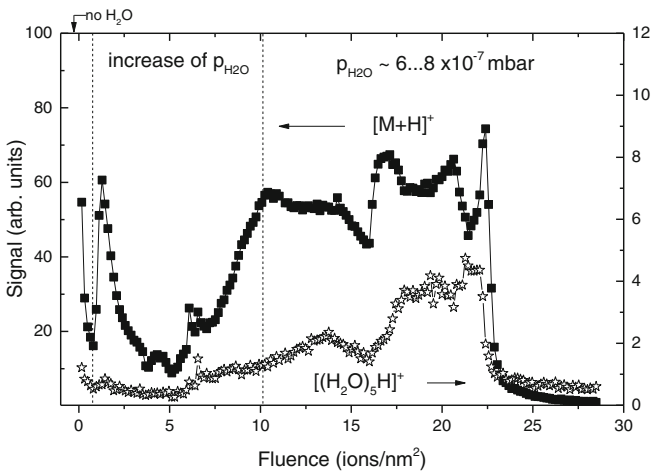

Figure 1. DRI depth profile of a 200 nm trehalose film on silicon using an HCl doped Ar_{1500}^+ (5% HCl) cluster beam under simultaneous adsorption of H_2O. Closed symbols: $[M + H]^+$ protonated molecule signal at *m/z* 343; open symbols: water cluster ion signal at *m/z* 91

As a result, the largest useful yield of all molecule-specific ions is obtained for the $[M – OH]^+$ fragment ion using C_{60} projectiles. Small bismuth or gold clusters, as predominantly used for data acquisition in many modern commercial ToF-SIMS instruments, generate this fragment ion at comparable but slightly lower useful yield values, whereas bare Ar clusters apparently do not ionize very well and exhibit useful yields that are at least an order of magnitude lower. If the comparison is restricted to the formation of the protonated molecule $[M + H]^+$, the picture changes. Here, the small metal cluster projectiles generate useful yield values, which are by an order of magnitude lower than those obtained with C_{60}. Pure Ar clusters perform even worse, and it is this situation we want to improve by incorporating reactive species into the cluster projectile. The data show that DRI may indeed increase the useful yield to a similar level as observed with C_{60}^+. It should be noted that a similar ionization efficiency can be obtained by adding NaCl to the trehalose film and monitoring the $[M + Na]^+$ sodium adduct ion [17]. As shown by the Vickerman group, a pure water cluster ion beam may generate a similar enhancement of the protonation efficiency compared with Ar clusters, reaching a

Table 1. Useful yield of molecule-specific secondary ions measured under bombardment of trehalose with different cluster projectile ions. The values were calculated from the published ToF-SIMS molecular depth profile data (see references) as described in the text

	Bi_3^+	C_{60}^+	Ar_n^+	*DRI*	$(H_2O)_n^+$
$[M – OH]^+$	4×10^{-6}	8×10^{-6} [8]	5×10^{-7}	2×10^{-6}	6×10^{-6}
$[M + H]^+$	2×10^{-7}	2×10^{-6}	9×10^{-8}	2×10^{-6}	6×10^{-6}
$[M – H]^-$		5×10^{-7}	4×10^{-6}	3×10^{-8}	

useful yield, which even exceeds that obtained with C_{60} [26]. In the negative ion spectrum, the $[M-H]^-$ deprotonation efficiency obtained with Ar clusters is significantly larger than that obtained with C_{60} and reaches values comparable to the protonation efficiency under optimized ionization conditions. The deprotonation efficiency obtained under DRI conditions is rather small, since in this case the DRI modality acts to shift the main ionization channel towards the $[M+Cl]^-$ adduct ion formation. Again, the useful yield of $[M+Cl]^-$ obtained under optimized DRI conditions is comparable to that obtained for $[M+H]^+$ formation.

Interestingly, none of the diverse efforts to enhance the chemical ionization of sputtered molecules that have been published so far has been able to push the useful yield of trehalose molecules above a value of the order of 10^{-5}. This observation suggests that in this case, the observed useful yield might not be limited by a poor ionization efficiency alone. Instead, it is speculated that there might be other effects, such as, for instance, a relatively efficient fragmentation of the sputtered molecules, which limits the useful yield for this system.

2. Irganox The Irganox multilayer system investigated here is similar to that used in a recent VAMAS round-robin study conducted by NPL [27]. We will, therefore, organize the discussion of the measured depth profiles along the lines outlined previously. Here we focus on the molecular ions, i.e., the protonated or deprotonated molecules $[M+H]^+$ and $[M-H]^-$ of 1098 (*m/z* 637 and 635) and 1010 (*m/z* 1178 and 1176), respectively. These ions have been shown to exhibit the most pronounced matrix effect [27]. For clarity, we will in the following show linear plots of these signals only. For reference to the behavior of different fragment or substrate related ions, each of the following Figures is accompanied by a corresponding Figure in the Supporting Information, which shows a logarithmic plot of major fragment signals along with a few additional ions related to water clusters or the substrate underlying the multilayer film.

In the absence of matrix effects, and under steady state sputtering conditions, the signal measured for a component *i* should be given as

$$I_i(\varphi) \propto \varphi_i \cdot Y(\varphi_i) \tag{1}$$

where I_i denotes the measured signal, φ_i denotes the concentration (or volume fraction) of species *i* in the sample, and *Y* denotes the sputter yield (i.e., the average number of molecule equivalents removed per projectile impact. The proportionality factor in Equation (1) is the absolute sensitivity factor, which includes the survival probability of a sputtered molecule against fragmentation, its ionization probability during the emission event, along with an instrumental detection efficiency of the emitted secondary ion. It is important to realize that this quantity only remains constant during the acquisition of a depth profile, if all three of the contributing factors do not change as a function of the sample composition. In addition, it is of note that the sputter yield will, in general, also depend on the composition, particularly in cases where the pure components exhibit significantly different yields and, therefore, cannot a priori be assumed to remain constant either. Only in cases where neither the absolute sensitivity factor nor the sputter yield vary as a function of composition, Equation (1) reduces to

$$I_i(\varphi_i) = \varphi_i \cdot I_1^i, \tag{2}$$

with I_1^i being the signal measured for a pure layer of species *i*. In the case of a molecular depth profile, another peculiarity arises from the fact that there may be crosstalk between different components. Other species present in the sample might contribute to the signal at the molecular ion mass of species *i*, which must be subtracted from $I_i(\varphi_i)$ in order to quantify the depth profile. In the two component system studied here, the background signal I_0^i generated by the pure film of the second component, corresponding to $\varphi_i = 0$, can be used. Using the corrected intensity $I_i(\varphi_i) - I_0^i$, Equation (2) forms the basis of the discussion in ref. [27]. Moreover, in cases where the sputter yield changes as a function of composition, Equation (2) can still be used to define a relative sensitivity factor RSF_i^j as the ratio of the absolute sensitivity for species *i* to that of a reference component *j*. Following the protocol outlined previously [27], we assume that the sputter yield remains constant for the Irganox1098/Irganox1010 layer system but we will cross-examine that assumption later and quantify the deviation from the ideal behavior of Equation (2) by calculating the matrix effect magnitude as

$$\Xi_i = 2\int_0^1 \frac{I_i(\varphi_i) - I_0^i}{I_1^i - I_0^i} d\varphi_i - 1 = 2\int_0^1 N_i(\varphi_i) d\varphi_i - 1, \tag{3}$$

with $\Xi = 0$ indicating ideal (matrix effect free) behavior, $\Xi < 0$ indicating suppression and $\Xi > 0$ indicating enhancement of the secondary ion formation for component *i*. For the two-component multilayer sample, there is only one value of $\varphi_i = 0.5$ within layer 2 in addition to the pure layers with $\varphi_i = 1$ for *i* =Irganox 1098 (layers1 and 3) and Irganox 1010 (layer 4), respectively. We therefore approximate the integral in Equation (4) by a polygon yielding

$$\int_0^1 N(\varphi) d\varphi \simeq \frac{1}{4} + \frac{1}{2} N\left(\frac{1}{2}\right) \quad and \quad \Xi = N\left(\frac{1}{2}\right) - \frac{1}{2} \tag{4}$$

using the normalized intensity $N(\varphi) = (I(\varphi) - I_0)/(I_1 - I_0)$ as introduced previously [27].

C_{60} Projectiles

For reference, we begin the discussion with a depth profile measured using a 40 keV C_{60}^+ ion beam. A plot of the relevant positive and negative secondary ions (i.e., the protonated or

deprotonated parent molecule of 1098 and 1010, respectively) versus the applied ion fluence is depicted in Figure 2. From a visual inspection of the data, it is seen that the negative secondary ions reflect the true composition of the sample, whereas the positive ions exhibit an extreme matrix effect in the sense that the sensitivity factor of the 1098 molecule must be enhanced by the presence of 1010. As a consequence, the negative spectrum resolves all four layers of the sample with the expected dip of the 1098 intensity within layer 2 to nearly half of that measured in the pure 1098 layers (layer 1 and 3), accompanied by nearly half the 1010 signal in layer 2 compared with the pure 1010 layer (layer 4). Quantification of this profile is easy and yields normalized intensities $N_{1098}\left(\frac{1}{2}\right) = 0.64$ and $N_{1010}\left(\frac{1}{2}\right) = 0.34$, resulting in $\Xi_{1098} = +0.14$ and $\Xi_{1010} = -0.16$. In other words, the 1098 intensity is slightly enhanced by the presence of 1010, whereas that of 1010 is slightly suppressed by the presence of 1098. The matrix effect is weak. The fact that both values of Ξ are nearly identical indicates that there is a constant RSF between the two components, leading to a linear correlation between both signals.

The positive spectrum, on the other hand, reflects a strong matrix effect in the sense that the 1098 signal does not drop at all in layer 2, indicating that the formation of this ion must be strongly enhanced by the presence of 1010. On the other hand, the 1010 signal appears to be higher in the pure 1098 layers than in the 1010-containing layer 2, indicating strong crosstalk between both components. As a consequence, the layer structure cannot be resolved and the profile is not quantifiable, formally giving a normalized intensity $N_{1098}\left(\frac{1}{2}\right) = 1.05$ corresponding to $\Xi_{1098} = +0.55$, while the normalized intensity of 1010 would be negative.

Pure Ar Cluster Projectiles

As the next step, we examine the depth profile measured with a pure Ar GCIB as shown in Figure 3. In both the positive and negative secondary ion mode, the 1098 profile obviously cannot be quantified since there is a signal increase between the first pure 1098 layer and the second mixed layer. This result is similar to that observed in the positive spectrum under C_{60} bombardment. Interestingly, both the protonation and the deprotonation efficiency of the 1098 molecule must, therefore, be significantly enhanced by the presence of 1010. From the 1010 signal, on the other hand, all four layers can be identified in the negative mode, while this is again not possible in the positive mode. From the absence of a positive 1010 signal rising above the 1098-induced crosstalk background, we find that the reduced intensity of this signal must be limited to $N_{1010} < 0.06$, yielding $\Xi_{1010}{}^{+}$ in excess of –0.44, whereas the resulting value for the negative 1010 signal is much better. Interestingly, this signal increases during removal of both the intermixed layer 2 (+18%) and the pure layer 4 (+44%). This increase, which is also observed with a HCl doped cluster ion beam (see below), also appears in the positive mode and is clearly reproducible. We will come back to this observation shortly. Since the signal in layer 4 is not constant, it is not clear where the reference value $I_1{}^{1010}$ needed for quantification should be taken. As a result, we arrive at a possible range $\Xi_{1010}{}^{-} = 0.14 \ldots 0.18$ depending upon whether the reference signal is taken at the end or the beginning of this layer.

The positive ion spectrum again shows a rise of the 1098 signal within the intermixed layer 2, yielding a normalized intensity that cannot be quantified and is associated with $\Xi_{1098}{}^{+}$ in excess of 0.5. The behavior of the negative ion 1098 signal appears erratic, showing a steep increase at the interface between layers 1 and 2 (corresponding to $\Xi_{1098}{}^{-} \simeq$

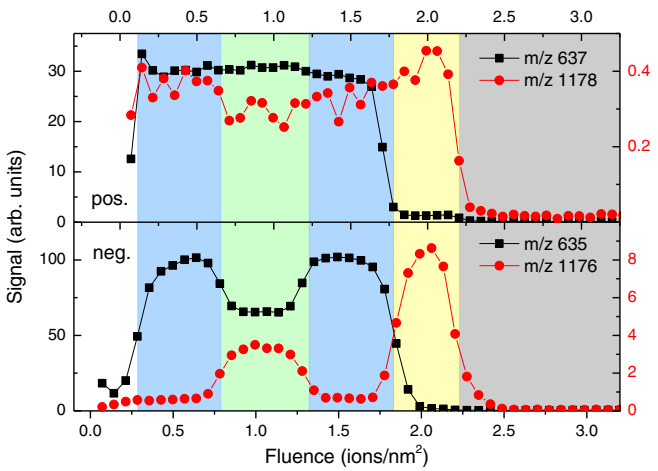

Figure 2. Depth profile of the positive $[M + H]^+$ and negative $[M - H]^-$ molecular secondary ions of Irganox 1098 (*m/z* 637 and 635) and Irganox 1010 (*m/z* 1178 and 1176) across the NPL irganox multilayer measured with a 20 keV $Ar_{3k}{}^{+}$ ion beam applied for erosion and data acquisition. For a logarithmic plot of all recorded signals see supporting Fig. S4

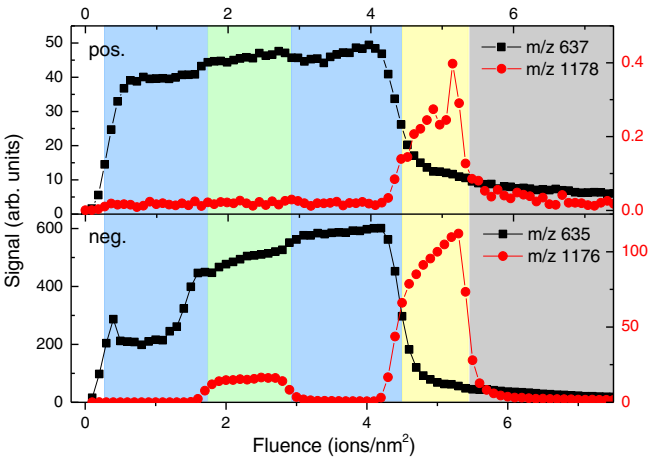

Figure 3. Depth profile of the positive $[M + H]^+$ and negative $[M - H]^-$ molecular secondary ions of Irganox 1098 (*m/z* 637 and 635) and Irganox 1010 (*m/z* 1178 and 1176) across the NPL irganox multilayer measured with an HCl doped 20 keV $Ar_{3k}{}^{+}$ (1.25% HCl) cluster ion beam applied for erosion and data acquisition. For a logarithmic plot of all recorded signals see supporting Fig. S5

1.60) and another increase at the second interface (corresponding to $\Xi_{1098}^- \simeq 0.40$). There are two possible explanations for this increase. Either the signal variation is influenced by an instrumental artifact, for instance a variation of the charge compensation efficiency due to the decreasing distance to the underlying substrate, or the matrix effect is extremely large in this case, leading to a strong signal increase as soon as the first 1010 containing second layer is reached. Since there will always be a residual 1010 content throughout the removal of the following third layer induced by interface mixing, this may suffice to keep the deprotonation efficiency of the 1098 molecule high, leading to a higher signal level. At present, we cannot clearly differentiate between these two possibilities, but we note that in the former case, the apparent reproducibility of the effect would appear surprising.

HCl Doped Ar Cluster Projectiles

Depth profiles measured with the HCl doped GCIB are shown in Figure 4. The first observation is that the signal levels obtained with these projectiles are practically identical to those obtained with the pure Ar GCIB. Again, it is seen that the negative ion spectrum allows a clear identification of all four sample layers, whereas the positive spectrum cannot be quantified. Although the profiles look somewhat similar to those obtained under bombardment with pure Ar clusters as shown in Figure 3, there are distinct differences that are noteworthy. First, the matrix effect observed for the positive ion 1098 signal is reduced, since the signal does not increase in the mixed layer 2. Based upon the interfaces shown in the negative ion mode, it appears there is a slight signal decrease in this layer, leading to a Ξ_{1098}^+ value slightly below +0.5. Second, the profile obtained in negative ion mode is improved over that measured under pure Ar cluster bombardment. The expected signal variation is similar to that observed under C_{60} bombardment. A detailed analysis of the normalized intensities observed in layer 2 yields $\Xi_{1098}^- = +0.28$ and $\Xi_{1010}^- = -0.11 \ \ldots \ -0.15$, the latter again depending on where in layer 4 the 1010 reference signal is taken. As already observed under pure Ar cluster bombardment, the 1010 signal increases during removal of both the intermixed layer 2 (+27%) and the pure layer 4 (+42%), indicating an enhancement of either the deprotonation probability or the partial molecule sputter yield which might be induced by the approaching substrate interface. In view of the latter, one could either imagine an enhancement of the total sputter yield (which would equally influence all measured signals) or a decreased fragmentation probability of the sputtered molecules. Inspection of the mass spectra reveals that all recorded fragment signals as well as the $[M + Cl]^-$ chlorine adduct ion signal exhibit the same variation (see Supporting Figure S5 for details), so that the most likely cause of the observed signal rise is an increase in the total sputter yield as the interface to the underlying silicon substrate is approached.

HCl Doped Ar Clusters and H_2O Adsorption

As the next step, we discuss the merits of the DRI scheme by combining the HCl doped Ar GCIB bombardment with the simultaneous adsorption of H_2O onto the sample surface from a controlled water vapor atmosphere. By monitoring the water cluster ion signals in the SIMS spectrum and carefully controlling the H_2O partial pressure to keep these signals constant, it is possible to obtain a depth profile under dynamically maintained reactive ionization conditions, as already shown in

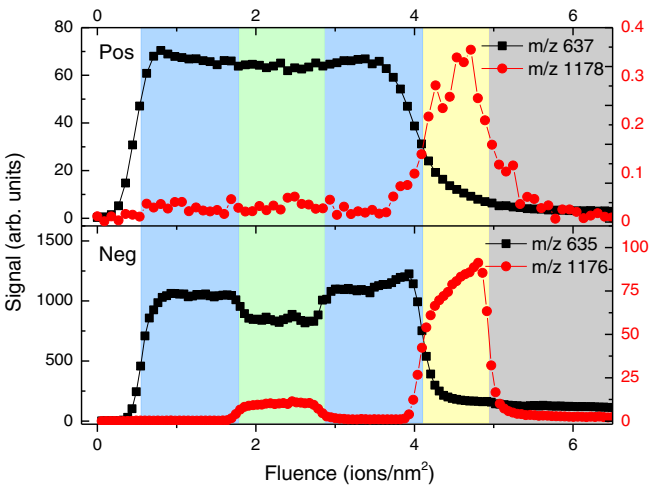

Figure 4. DRI depth profile of the positive $[M + H]^+$ and negative $[M - H]^-$ molecular secondary ions of Irganox 1098 (*m/z* 637 and 635) and Irganox 1010 (*m/z* 1178 and 1176) across the NPL irganox multilayer measured with an HCl doped 20 keV Ar_{3k}^+ (1.7% HCl) cluster ion beam under simultaneous H2O adsorption from a controlled water vapor atmosphere. For a logarithmic plot of all recorded signals see supporting Fig. S6

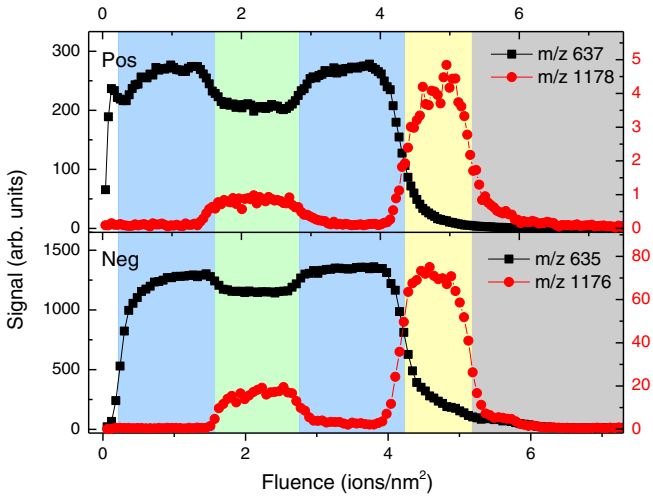

Figure 5. DRI depth profile of the positive $[M + H]^+$ and negative $[M - H]^-$ molecular secondary ions of Irganox 1098 (*m/z* 637 and 635) and Irganox 1010 (*m/z* 1178 and 1176) across the NPL Irganox multilayer measured with an HCl doped 20 keV Ar_{3k}^+ (1.7% HCl) cluster ion beam under simultaneous H_2O adsorption from a controlled water vapor atmosphere. For a logarithmic plot of all recorded signals see Supporting Figure S6

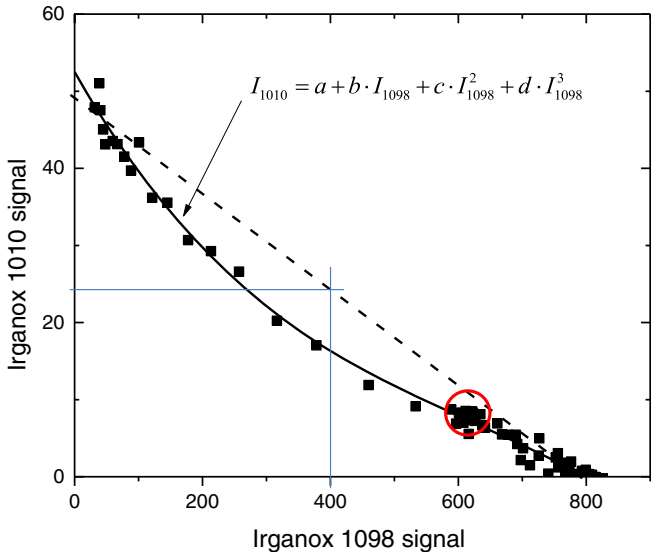

Figure 6. Correlation plot of positive $[M + H]^+$ secondary ions of Irganox 1098 (*m/z* 637) and Irganox 1010 (*m/z* 1178) depicted in Figure 5. The solid line represents a fit to the data according to the formula given in the Figure

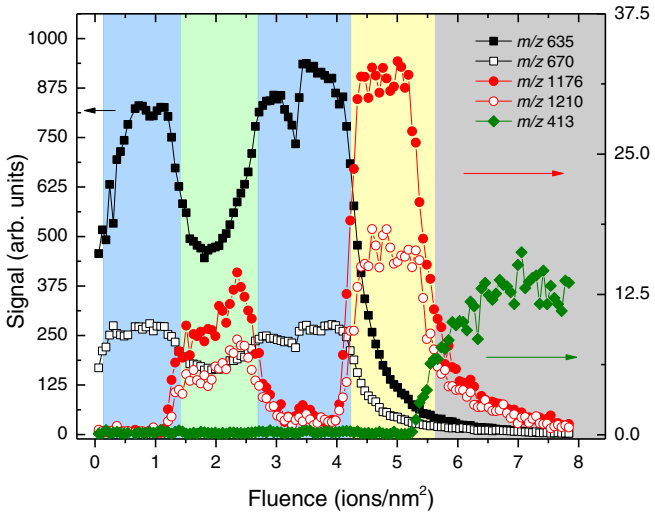

Figure 7. DRI depth profile of the negative $[M - H]^-$ (*m/z* 635 and 1176) and $[M + Cl]^-$ (*m/z* 670 and 1210) secondary ions representing the Irganox 1098 and Irganox 1010, respectively, measured with an HCl doped 20 keV Ar_{3k}^+ (1.25% HCl) cluster ion beam under simultaneous H_2O adsorption from a controlled water vapor atmosphere. The H_2O partial pressure was doubled compared with that in the lower panel of Figure 5

Figure 1. This strategy was employed to depth profile the NPL Irganox multilayer sample as shown in Figure 5. The most notable difference to the data presented in Figures 2–4 is the fact that all four layers of the sample can be identified in positive ion mode. Moreover, the signal levels in the positive ion spectrum are drastically increased, whereas those of the negative ions remain virtually unchanged. Both findings are expected, since the projectile assisted surface chemistry induced by the reaction of HCl entrained in the projectile with the adsorbed H_2O molecules leads to the production of $(H_2O)H^+$ ions, thereby improving the protonation efficiency while leaving the deprotonation efficiency unchanged [17]. It should be noted that if the same experiment is repeated with a pure Ar GCIB under simultaneous H_2O flooding conditions, the resulting profiles look virtually identical to those obtained without any water/ice coverage as presented in Figure 3. Hence, the signal enhancement must be caused by the reactive ionization effect. If corrected for differences in primary ion current, the magnitude of the increase is ~4× (1098) and ~15× (1010), thereby boosting the 1010 signal to roughly the same relative level (several percent) compared with the 1098 ion signal as observed in the negative spectrum. This finding shows that the relatively low 1010 signal observed in the positive ion spectrum under pure Ar GCIB bombardment must in part be due to incomplete ionization of sputtered intact 1010 molecules. Moreover, the fact that under DRI conditions both ionization modes yield similar signal ratios suggests that the still lower signal measured for 1010 may in part be caused by fragmentation of the larger 1010 molecule compared with its smaller 1098 counterpart rather than inefficient ionization.

Under DRI conditions, it is now possible to quantify the positive ion profile. From the data in the upper panel of Figure 5, the normalized intensities are $N_{1098} = 0.76$ and $N_{1010} = 0.18$ in the intermixed layer, leading to $\Xi_{1098}^+ = +0.26$ and $\Xi_{1010}^+ = -0.32$. Even though the DRI modality improves the quantifiability of the profile, there is still a remaining matrix effect, which can be seen by the nonlinear correlation between both signals as shown in Figure 6. Specifically, note that the data points circled in the Figure correspond to the intermixed layer with 50% stoichiometry. In the absence of matrix effects, these points should be located in the center of the straight line as indicated in the Figure.

For the negative ion profile in Figure 5, there is a less favorable situation with normalized intensity values of $N_{1098} = 0.88$ and $N_{1010} = 0.22$ in the intermixed layer, yielding $\Xi_{1098}^- = +0.33$ and $\Xi_{1010}^- = -0.28$, respectively. If analyzed under comparable DRI conditions, the positive ion spectrum provides a quantitatively better representation of the intermixed layer stoichiometry than the negative ion spectrum, a finding which is in contrast to all other analysis conditions explored in the VAMAS round-robin study of this material [27]. It is a clear indication that the reactive ionization enhancement via HCl induced surface chemistry is effective, since this approach is specifically designed to boost the positive ionization via protonation of a sputtered molecule.

An interesting question regarding the DRI protocol is how the ionization efficiency depends upon the HCl content in the projectile and/or the water/ice coverage of the surface. In order to investigate this question, depth profiles were taken at different HCl doping levels using the same partial H_2O pressure during the analysis. The results are shown in the Supporting Information (Supporting Figure S7) and reveal that both the signal level and the quality of the depth profile decrease if the dopant level is increased. In fact, we find an HCl content of about 1% to 2% in the expansion gas forming the cluster ion

beam to yield optimum DRI conditions. At this level, we observe that higher water vapor pressure tends to improve the quality of the depth profile. As an example, depth profiles of the negative quasimolecular ions $[M - H]^-$ and $[M + Cl]^-$ are shown in Figure 7, which were recorded using the same dopant level as employed for the profile shown in Figure 5, albeit at a higher H_2O partial pressure leading to a higher water/ice surface coverage. It is seen that the quality of the depth profile with regard to quantitation is improved, yielding normalized intensity values of $N_{1098} = 0.54$ and $N_{1010} = 0.28$ … 0.44 in the intermixed layer, the latter depending on where exactly the signal is taken in the slightly sloping signal gradient observed in layer 2. These values correspond to $\Xi_{1098}^- = +0.04$ and $\Xi_{1010}^- = -0.06$ … 0.22 and represent the closest approximation of the true layer stoichiometry that could be achieved in this work. From these observations, we conclude that higher water/ice coverage improves the dissociation efficiency of the HCl molecules entrained in the projectile, as would be expected from basic chemistry reaction dynamics. On the other hand, we note that care must be taken when increasing the H_2O partial pressure during the analysis in order to avoid the accumulation of an ice overlayer on the surface. The water/ice coverage is determined by an equilibrium between deposition and sputter removal of water molecules. The former is governed by the H_2O partial pressure and the surface temperature, the latter critically depends on the sputter yield. Particularly in cases where the sputter rate of water ice is slower than that of the organic film, ice patches will accumulate at the surface as soon as the equilibrium H_2O surface concentration of 1 is reached. In these patches, erosion will slow down and a net deposition of ice will occur. As a consequence, the dynamic equilibrium is lost and the surface starts to be covered with a strongly inhomogeneous, growing ice film. In this case the useful molecular ion signals and the observed depth resolution are degraded. It is clear that this situation must be avoided, even if this may lead to a slightly less than optimal reactive ionization efficiency.

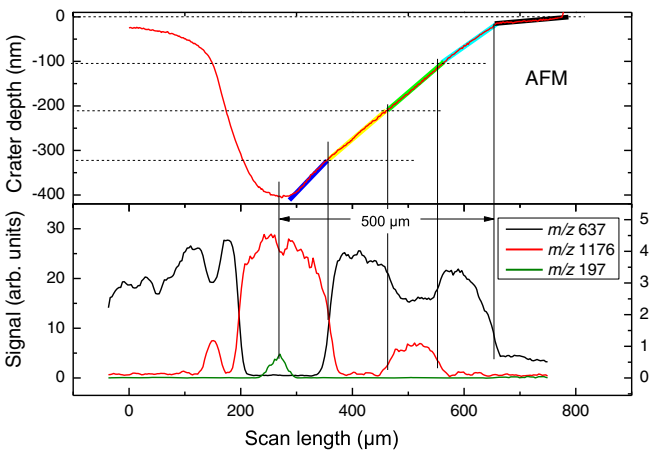

Figure 8. Top panel: line scan across an AFM image of a wedge crater eroded into the Irganox multilayer film using a 20 keV Ar_{3k}^+ cluster ion beam. Bottom panel: line scan across a SIMS image of the wedge crater taken with a 40 keV C_{60}^+ ion beam

Sputter Yields

The sputter yield volume (i.e., the sample volume removed per projectile ion impact) is easily derived from a depth profile across a film of known thickness, provided the interface between the film and the surrounding material can clearly be identified. In order to determine the individual layer thicknesses in NPL sample, a wedge crater was eroded into the film using the pure Ar cluster ion beam. The rationale behind this approach is that variations of the erosion rate as a function of depth can be detected on this way as a varying slope of the wedge shaped crater bottom [24, 25]. An AFM image of the resulting crater is shown in the Supporting Figure S8. A line scan perpendicular to the wedge direction (indicated by the white line) yields a total crater depth of 420 nm. Since the silicon substrate is not significantly eroded by the Ar cluster ion beam, this depth therefore corresponds to the total thickness of the Irganox multilayer film. From Figure 3, it is seen that an Ar_{3000}^+ ion fluence of about 5 ions/nm^2 is needed to remove the film, corresponding to an average sputter yield volume of ~84 nm^3. This value is, by a factor 2.4, smaller than the yield measured under 40 keV C_{60}^+ bombardment, as seen by comparing the profiles shown in Figure 2 and Figure 3. A line scan along the wedge direction is shown in the upper panel of Figure 8. It is seen that the slope of the curve indeed varies, as indicated by the thick lines underlying the data. This variation allows determination of the relative erosion rate of the different layers. First, it is noted that the sample must have been covered by a thin layer of about 10 nm thickness, which is eroded extremely slowly. We presume that this is caused by a surface oxide layer or an ice overlayer that had been formed on the cold sample surface prior to the analysis due to the water desorption process by warming the sample to –120 °C and recooling the sample. In the DRI experiment, the result of which is presented in Figure 5, the water doping and SIMS acquisition started at the same time at the optimized the equilibrium condition; therefore, no water condensation was on the sample surface.

In order to verify the layer identification, a SIMS image of the wedge crater was acquired in negative secondary ion mode using the C_{60}^+ ion beam, and a line scan across that image was performed along the same wedge direction as the AFM scan. The result of this analysis is shown in the bottom panel of Figure 8. It is seen that the interfaces between the different

Table 2. Thickness and sputter yield volume under bombardment with 20 keV Ar_{3k}^+ cluster ions determined for the individual layers of the irganox multilayer sample as described in the text

	Film thickness (nm)	*Sputter yield (nm^3)*	
		20 keV Ar_{3k}^+	40 keV C_{60}^+
Layer 1 (1098)	105	78	198
Layer 2 (1098/1010)	105	88	202
Layer 3 (1098)	106	77	186
Layer 4 (1010)	104	113	242

layers, which are marked by vertical lines, allow a precise definition of the layer boundaries in the AFM scan. Moreover, the SIMS data confirm that the shallow surface overlayer identified in the AFM data indeed exists and shows a very low SIMS signal as well. The thickness of the individual layers of the Irganox multilayer sample, which was determined from this analysis, is shown in Table 2. By converting the different slopes indicated in Figure 8 into an erosion rate, the sputter yields for the different layers can be calculated as listed in Table 2 along with the related individual layer thickness. The first observation is that all four layers appear to have roughly the same thickness of about 105 nm, which was targeted by the film deposition process. Moreover, the AFM data reveal that the assumption of a constant sputter yield throughout the depth profile is incorrect. While the pure 1098 layers (layers 1, 3) and the intermixed layer (layer 2) exhibit a similar sputter yield, the erosion rate of the pure 1010 layer (layer 4) appears to be significantly larger. This finding is consistent with the observation in the depth profiles, which consistently show that the removal of this layer requires about 33% less ion fluence than that required to remove the first three layers. Interestingly, this difference is not as pronounced in the depth profiles obtained under C_{60}^+ ion sputtering, indicating that in this case the sputter yields of Irganox 1098 and Irganox 1010 are closer.

These observations bear an important consequence regarding the quantitation of the measured signals. Following Equation (1), the relative intensities measured in layer 4 must be corrected for the enhanced sputter yield and, hence, scaled down by about 34% before being compared with the signals measured in the remaining layers. As a consequence, the normalized 1010 intensity N_{1010} calculated for the intermixed layer is increased, leading to a more quantitative representation of the layer stoichiometry. For the depth profile analysis performed under DRI conditions, this results in a residual matrix effect magnitude of $\Xi_{1098}{}^+ = +0.26$ and $\Xi_{1010}{}^+ = -0.26$ in the positive ion spectrum (upper panel of Figure 5) and $\Xi_{1098}{}^- = +0.04$ and $\Xi_{1010}{}^- = -0.04$ in the negative spectrum (Figure 7).

Conclusions

The experiments performed here demonstrate that the DRI modality can successfully be employed to enhance the ionization probability of molecule-specific secondary ions via protonation or deprotonation of intact sputtered target molecules. As a result, a more uniform ionization efficiency among different molecules is obtained, leading to a reduction of intermolecular matrix effects, particularly when depth profiling is performed in the positive ion mode. The data show that it is possible to dynamically establish and maintain optimum conditions to tune the surface chemistry between reactive species (here: HCl) entrained in the cluster projectile and a water/ice coverage throughout an entire depth profile across an organic multilayer film of about half a micrometer thickness. In the particular example studied here, DRI yields improved molecular depth profiles on the NPL multilayer system, which are otherwise not quantitatively interpretable. Using the DRI modality, all different layers of the sample can clearly be identified and reasonably characterized according to their stoichiometric composition both in the positive and in the negative secondary ion spectrum. This task is impossible when using a pure Ar GCIB for sputtering and data acquisition. In particular, we find that the DRI

- leaves the sputter yield obtained with an Ar cluster ion beam unchanged, as long as the buildup of a thick ice overlayer is avoided;
- enhances the signal level of protonated molecules $[M + H]^+$ by factors of 4× (1098) and 15× (1010) compared with pure Ar cluster projectiles, and by a factor of 5× with respect to that obtained under bombardment with C_{60}^+ ions of twice the impact energy;
- provides a more uniform ionization efficiency between different molecules that cannot be obtained under pure Ar cluster ion bombardment, and hence
- renders an otherwise uninterpretable molecular secondary ion depth profile taken in the *positive* ion mode interpretable in a quantitative manner.

The data also show that the quantification of depth profiles taken in the *negative* ion mode may benefit from the projectile induced surface chemistry. Using the DRI scheme in connection with a relatively large H_2O surface concentration, we obtain an almost matrix effect-free representation of the intermixed Irganox 1098/1010 layer, which outperforms the result obtained with C_{60}^+ projectiles.

Acknowledgment

The authors gratefully acknowledge the National Institutes for Health grant 5R01GM113746 - 21. The support from Novartis is also appreciated.

References

1. Deline, V.R., Katz, W., Evans, C.A., Williams, P.: Mechanism of the SIMS matrix effect. Appl. Phys. Lett. **33**, 832–835 (1978)
2. Sykes, D.E., Chew, A., Crapper, M.D., Valizadeh, R.: The effect of oxygen flooding on the secondary ion yield of Cs in the Cameca IMS 3f. Vacuum **43**, 159–162 (1992)
3. Kasel, B., Wirtz, T.: Reduction of the SIMS matrix effect using the storing matter technique: a case study on Ti in different matrices. Anal. Chem. **86**, 3750–3755 (2014)
4. Meyer, K., Hagenhoff, B., Deimel, M., Benninghoven, A., Bauch, H.J.: Quantification of molecular secondary ion mass spectrometry by internal standards. Org. Mass Spectrom. **27**, 1148–1150 (1992)
5. Shard, A.G., Foster, R., Gilmore, I.S., Lee, J.L.S., Ray, S., Yang, L.: VAMAS interlaboratory study on organic depth profiling. Part I: Preliminary report. Surf. Interface Anal. **43**, 510–513 (2011)
6. Facchetti, A.: Organic semiconductors: made to order. Nat. Mater. **12**, 598–600 (2013)
7. Kraft, M.L., Klitzing, H.A.: Imaging lipids with secondary ion mass spectrometry. Biochim. Biophys. Acta **1841**, 1108–1119 (2014)
8. Cheng, J., Wucher, A., Winograd, N.: Molecular depth profiling with cluster ion beams. J. Phys. Chem. B **110**, 8329–8336 (2006)

9. Fletcher, J.S., Conlan, X.A., Lockyer, N.P., Vickerman, J.C.: Molecular depth profiling of organic and biological materials. Appl. Surf. Sci. **252**, 6513–6516 (2006)
10. Winograd, N.: Molecular depth profiling. Surf. Interface Anal. **45**, 3–8 (2013)
11. Mahoney, C.M., Roberson, S., Gillen, G.: Dynamic SIMS utilizing SF5+ polyatomic primary ion beams for drug delivery applications. Appl. Surf. Sci. **231/232**, 174–178 (2004)
12. Weibel, D., Wong, S., Lockyer, N., Blenkinsopp, P., Hill, R., Vickerman, J.C.: A C60 primary ion beam system for time of flight secondary ion mass spectrometry: its development and secondary ion yield characteristics. Anal. Chem. **75**, 1754–1764 (2003)
13. Yamada, I., Matsuo, J., Toyoda, N., Kirkpatrick, A.: Materials processing by gas cluster ion beams. Mater. Sci. Eng. R **34**, 231–295 (2001)
14. Nojima, M., Suzuki, M., Fujii, M., Seki, T., Matsuo, J.: Development of organic SIMS system with Ar-GCIB and IMS-4f. Surf. Interface Anal. **46**, 368–371 (2014)
15. Vickerman, J.C., Briggs, D.: ToF-SIMS: Surface Analysis by Mass Spectrometry (2nd ed.). SurfaceSpectra/IM Publications, West Sussex/Manchester, UK (2013)
16. Sheraz née Rabbani, S., Barber, A., Fletcher, J.S., Lockyer, N.P., Vickerman, J.C.: Enhancing secondary ion yields in time of flight-secondary ion mass spectrometry using water cluster primary beams. Anal. Chem. **85**, 5654–5658 (2013)
17. Tian, H., Wucher, A., Winograd, N.: Dynamic reactive ionization with cluster secondary ion mass spectrometry. J. Am. Soc. Mass Spectrom. **27**, 285–292 (2015)
18. Tian, H., Wucher, A., Winograd, N.: Reduce the matrix effect in biological tissue imaging using dynamic reactive ionization and gas cluster ion beams. Biointerphases **11**, 02A320 (2016)
19. Cheng, J., Winograd, N.: Depth profiling of peptide films with TOF-SIMS and a C60 probe. Anal. Chem. **77**, 3651–3659 (2005)
20. Shard, A.G., Spencer, S.J., Smith, S.A., Havelund, R., Gilmore, I.S.: The matrix effect in organic secondary ion mass spectrometry. Int. J. Mass Spectrom. **377**, 599–609 (2015)
21. Wucher, A., Tian, H., Winograd, N.: A mixed cluster ion beam to enhance the ionization efficiency in molecular secondary ion mass spectrometry. Rapid Commun. Mass Spectrom. **28**, 396–400 (2014)
22. Hill, R., Blenkinsopp, P., Thompson, S., Vickerman, J., Fletcher, J.S.: A new time-of-flight SIMS instrument for 3D imaging and analysis. Surf. Interface Anal. **43**, 506–509 (2011)
23. Poerschke, D., Wucher, A.: Depth profiling of anodic tantalum oxide films with gold cluster ions. Surf. Interface Anal. **43**, 171–174 (2011)
24. Mao, D., Lu, C.Y., Winograd, N., Wucher, A.: Molecular depth profiling by wedged crater beveling. Anal. Chem. **83**, 6410–6417 (2011)
25. Mao, D., Wucher, A., Winograd, N.: Molecular depth profiling with cluster secondary ion mass spectrometry and wedges. Anal. Chem. **82**, 57–60 (2010)
26. Rabbani, S.S.N., Razo, I.B., Kohn, T., Lockyer, N.P., Vickerman, J.C.: Enhancing ion yields in time-of-flight-secondary ion mass spectrometry: a comparative study of argon and water cluster primary beams. Anal. Chem. **87**, 2367–2374 (2015)
27. Shard, A.G., Havelund, R., Spencer, S.J., Gilmore, I.S., Alexander, M.R., Angerer, T.B., Aoyagi, S., Barnes, J.P., Benayad, A., Bernasik, A., Ceccone, G., Counsell, J.D.P., Deeks, C., Fletcher, J.S., Graham, D. J., Heuser, C., Lee, T.G., Marie, C., Marzec, M.M., Mishra, G., Rading, D., Renault, O., Scurr, D.J., Shon, H.K., Spampinato, V., Tian, H., Wang, F.Y., Winograd, N., Wu, K., Wucher, A., Zhou, Y.F., Zhu, Z.H.: Measuring compositions in organic depth profiling: results from a VAMAS interlaboratory study. J. Phys. Chem. B.**119**, 10784–10797 (2015)